THE ASTROPHYSICAL JOURNAL, 372:494–504, 1991 May 10

THE LOCAL INTERSTELLAR MEDIUM TOWARD THE CENTER OF LOOP I[1]

MIRIAM CENTURION[2]
Instituto de Astrofísica de Canarias

AND

GIOVANNI VLADILO
Osservatorio Astronomico di Trieste, Via G.B. Tiepolo 11 I-34131, Trieste, Italy
Received 1990 July 10; accepted 1990 October 18

ABSTRACT

We have analyzed optical and ultraviolet spectra of nearby stars ($r \leq 200$ pc) located within the area of Galactic coordinates $310° \leq l \leq 330°$ and $15° \leq b \leq 25°$, in a study of the LISM toward the center of Loop I. The optical spectra show a multiple-component structure, with one prominent absorption plus one or two weaker features. The weaker components generally have Na I/Ca II < 1. One of them is identified with the nearby ($d \leq 5$ pc) component *P* of Lallement, Vidal-Madjar & Ferlet. The most intense components generally have Na I/Ca II > 1, and show good velocity coincidence with the global flow derived by Crutcher. The analysis of the UV spectra reveals a sudden increase of the gas column density as a function of distance, from $N_{\rm H\,I} \simeq 10^{18}$ cm^{-2} to $\simeq 10^{20}$ cm^{-2}, suggesting the presence of a wall of gas at 40 ± 25 pc from the Sun. This result constrains the distance to the boundary of the Local Bubble—the soft X-ray emitting cavity around the Sun—in the direction toward the center of Loop I. At larger distances, the approximately constant $N_{\rm H\,I}$, and the lack of detection of new interstellar components in the optical spectra, suggest the presence of another cavity of very low-density gas, identified with the Loop I Bubble. Along a few lines of sight, we have been able to estimate the physical parameters of the gas located at the boundary between the Local Bubble and Loop I Bubble by means of an analysis of optical (Na I) and UV (Mg I, Zn II) species, under the assumption of ionization equilibrium. We find evidence of warm gas ($T \simeq 6$–7×10^3 K) in the direction of η Cen and ζ Cen, and of colder gas in front of HD 129685 and probably HD 119921. The electron densities of the warm gas in front of η Cen ($\simeq 0.03$ cm^{-3}) and ζ Cen ($\simeq 0.04$ cm^{-3}) are very similar to the space averaged densities derived by means of pulsar dispersion measures in the LISM. The fractional ionization of this gas is less than that predicted by McKee and Ostriker for the warm neutral phase of interstellar space.

Subject headings: interstellar: abundances — interstellar: matter — ultraviolet: spectra

1. INTRODUCTION

The local interstellar medium (LISM) is a convenient framework for studies of the general interstellar space, given its complex morphology as revealed by observations in different spectral ranges (for recent reviews see Paresce 1984; Cox & Reynolds 1987; Bruhweiler & Vidal-Madjar 1987). Backscattering observations of solar Lyα photons within the solar system (Bertaux 1984) and observations of Lyα absorptions toward nearby cool stars (Landsman et al. 1984) indicate that the Sun is embedded in a warm ($T \approx 10^4$ K), low-density ($n_{\rm H\,I} \approx 0.1$ cm^{-3}) gas with an extension of several parsecs. The presence of much hotter gas at greater distances is indicated by soft X-ray surveys (McCammon et al. 1983) and by the detection of O VI interstellar absorptions in some stars within 100 pc (Jenkins 1978). The soft X-ray background can be explained as thermal emission produced by a volume of hot gas ($T \simeq 10^6$ K) around the Sun, the Local Bubble, with a linear size of about 100 pc (Snowden et al. 1990). Nonthermal radio emission observations have shown the existence of a nearby circular structure, the Loop I, centered at $l \simeq 330°$ and $b \simeq +18°$ (Berkhuijsen, Haslam, & Salter 1971). The enhancement of the diffuse X-ray background in this general direction of the sky is consistent with the presence of a nearby bubble of hot gas, the Loop I Bubble (Iwan 1980). A scenario in which H I gas flows from the general direction of the center of Loop I, impelled by stellar winds and supernovae explosions, was proposed by Weaver (1979) on the basis of radio 21 cm and optical polarization observations. A kinematical analysis of optical interstellar absorptions within about 100 pc confirms that the Sun is immersed in a coherently moving material flowing from the direction of the Sco-Cen association (Crutcher 1982). On a smaller distance scale, Lallement, Vidal-Madjar, & Ferlet (1986, hereafter LVF) have detected four separate motions within $\simeq 20$ pc of the Sun, arguing that the global flow derived by Crutcher (1982) is a mean motion of a finer velocity structure.

Given the existence of all these interstellar constituents, a detailed study of the LISM can provide important tests for current ISM models (e.g., McKee & Ostriker 1977), and in particular for studying the geometrical distribution and the physical state of the different interstellar phases. The three-dimensional distribution of the soft X-ray absorbing gas in the LISM is of particular interest for testing the validity of the models reproducing the observed soft X-ray background (Cox & Reynolds 1987). A powerful technique for studying the three-dimensional distribution of the interstellar gas, and in particular of the LISM, consists in studying the absorption spectra of stars located at different distances within small areas of the sky. In this work we study the area within the Galactic

[1] Based on observations collected at the European Southern Observatory at La Silla (Chile) and on observations by the *IUE* satellite collected at the VILSPA station of the European Space Agency.

[2] At the present time Fellow at the Osservatorio Astronomico di Trieste. Postal address: Osservatorio Astronomico di Trieste, Via G.B. Tiepolo 11 I-34131, Trieste, Italy.

TABLE 1

TARGETS

HD	Name	V	Spectral Type	$V \sin i$ (km s^{-1})	l	b	r (pc)
115892....	ι Cen	2.75	A2 V	85	309°4	25°8	16
119921....	...	5.15	A0 V	437	315.3	25.3	74
121263....	ζ Cen	2.55	B2.5 IV	219	314.1	14.2	102
121743....	ϕ Cen	3.83	B2 IV	126	316.0	19.1	213
123139....	θ Cen	2.06	K0 IIIb		319.5	24.1	15
125473....	ψ Cen	4.05	A0 IV	101	321.7	21.7	59
127972....	η Cen	2.31	B1.5 IVne	333	322.8	16.7	130
129685....	...	4.92	A0 V	455	327.4	22.1	67

coordinates range $310° \leq l \leq 330°$ and $15° \leq b \leq 25°$. This field is of particular interest because it is angularly close to the center of Loop I and because it lies within the contours of several interstellar components proposed by LVF. The present study is based on optical and UV observations of nearby fast-rotating stars, described in § 2. The rotationally broadened spectra of these targets make it possible to detect sharp interstellar absorptions easily. The optical observations, performed at high spectral resolution (FWHM = 3–5 km s^{-1}), have been used to identify the absorption components on kinematical grounds and to study the Na I/Ca II ratios (§ 3). The ultraviolet observations, characterized by a lower resolution (FWHM $\simeq$ 20 km s^{-1}), have allowed us to measure the column densities of the most abundant interstellar species and to study the depth distribution of the gas (§ 4). Abundances of optical and UV species have been combined in order to cast light on the physical state of the interstellar components under study (§ 5).

2. OBSERVATIONS AND DATA REDUCTION

The stars observed are listed in Table 1 with their basic data, which are taken from the Bright Star Catalogue (Hoffleit & Jaschek 1982, hereafter BS). The distances, r, were calculated by using the unreddened distance modulus $V - M_V - 3 \times E(B-V)$ when $r > 30$ pc, and by means of trigonometric parallax for the remaining cases. The $(B-V)_0$ unreddened scale was taken from FitzGerald (1970) and the absolute magnitudes from Grenier et al. (1985) and Walborn (1972). In Figure 1 we show the projection on the sky of our targets. For the sake of comparison, in the same figure we show the nearby cool star θ Cen (r = 15 pc), for which the interstellar Mg II has been measured by our collaborators (Genova et al. 1990).

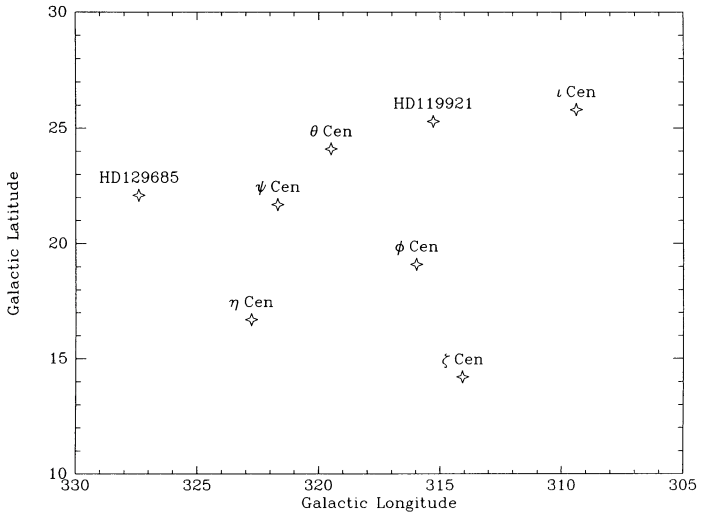

FIG. 1.—Projection on the sky of our targets in Galactic coordinates

The optical observations were performed at ESO (La Silla, Chile) in 1988 April by means of the Coudé echelle spectrograph (CES) fed by the 1.4 m telescope. Observations in the Na I region were performed at a spectral resolution $\lambda/\Delta\lambda \simeq 10^5$ using a Reticon detector. The Ca II spectral region was observed at $\lambda/\Delta\lambda \simeq 6 \times 10^4$ using a CCD detector. The log of the observations is shown in Table 2. Apart from the stars listed in Table 1, we have also observed the Na I spectrum of α Vir ($r \simeq 80$ pc), which is located at a higher Galactic latitude but in the same longitude range of our field.

The spectra were extracted, flat-fielded and calibrated in wavelength using standard IHAP commands (see IHAP User Manual, ESO 1983). A thorium lamp was used for the wavelength calibration, providing a dispersion curve with an internal accuracy of about 2 mÅ in the Na I region and $\simeq$3 mÅ in the Ca II region. A Na I spectrum of α Pic ($V \sin i$ = 205 km s^{-1}) was used as a template to eliminate telluric contamination. This star ($l = 272°$, $b = -24°$, r = 19 pc) was selected as a candidate free of interstellar absorptions, as it is located in a general direction of low density of interstellar gas in the LISM (Paresce 1984), and closer than the majority of the stars of our sample.

As far as the ultraviolet range is concerned, we analyzed 23 *International Ultraviolet Explorer* (*IUE*) spectra in the high-resolution mode ($\lambda/\Delta\lambda \simeq 2 \times 10^4$), partly in the short wavelength range (1250–2200 Å; SWP camera), and partly in the long wavelength range (2200–3000 Å; LWP camera). The available data are listed in Table 3. Some of the spectra, those indicated by an asterisk in the table, were obtained by our group. The others were obtained from the *IUE* data bank at VILSPA (Madrid). Owing to the limited dynamical range of the *IUE* cameras, we used, when possible, several spectra with

TABLE 2

OPTICAL OBSERVATIONS

HD	Range	t_{exp} (minutes)	Date
115892.....	Na I	6	1988 Apr 6
	Na I	12	1988 Apr 6
119921.....	Ca II K	60	1988 Apr 1
	Ca II H	60	1988 Apr 2
	Na I	60	1988 Apr 6
	Na I	90	1988 Apr 8
121263.....	Ca II K	6	1988 Apr 1
	Ca II H	6	1988 Apr 2
	Na I	15	1988 Apr 6
	Na I	15	1988 Apr 8
121743.....	Ca II K	18	1988 Apr 1
	Ca II H	18	1988 Apr 2
	Na I	30	1988 Apr 8
125473.....	Na I	5	1989 May 10
127972.....	Ca II K	5	1988 Apr 1
	Ca II H	5	1988 Apr 2
	Na I	10	1988 Apr 8
129685.....	Ca II K	50	1988 Apr 1
	Ca II H	70	1988 Apr 2
	Na I	50	1988 Apr 7
116658.....	Na I	4	1988 Apr 8
	Na I	2.5	1988 Apr 7

TABLE 3

IUE OBSERVATIONS

HD	SWP	LWP
115892.....	30010	9842
	30124	9964
	30532	10331
119921.....	20192[a]	16128[a]
	20854	
	22668	
121263.....	20363	8852
121743.....	21956	...
123139.....	...	4416[a]
125473.....	30544	10341
127972.....	18858	12286
	19613	
	20678	
129685.....	20193[a]	16129[a]
	20856	

[a] Our *IUE* observations.

different exposure levels for each star. All the data were calibrated by means of the standard IUESIPS package. To reduce the effect of high-frequency noise, we smoothed the original spectra by means of a three-point triangular filter.

All the interstellar absorptions, in the optical and in the UV, were normalized to the adjacent, slowly varying photospheric intensity (pseudocontinuum). Some examples of normalization are shown in Figure 2. After normalization, the typical rms of the continuum, σ_{con}, was used to estimate the signal-to-noise ratio, S/N = $1/\sigma_{con}$. Typical values of S/N are about 250 for Na I lines, between 250 and 350 for Ca II lines, and between 20 and 40 for the relevant spectral ranges in our *IUE* spectra. The S/N in the Na I range has been measured after correction for the telluric lines.

The line centers and equivalent widths have been measured by means of Gaussian fits in the normalized spectra. Some examples of fits are shown in Figure 3. Errors in the equivalent widths have been derived by adding up in quadrature the statistical errors and the uncertainty in the continuum tracing. The statistical errors have been estimated using the procedure of Jenkins et al. (1973). The uncertainty on the continuum placement was quantified by increasing and decreasing the continuum level by 1 σ_{con} and remeasuring the equivalent widths in each case. Upper limits for undetected features were derived by using the minimum detectable equivalent width, $W_{min} = 3\sigma_{con}\Delta\lambda_{instr}$, where $\Delta\lambda_{instr}$ is the FWHM of the instrumental profile. Column densities were derived by means of the theoretical, single-component curve of growth (Unsöld 1955, pp. 288–293).

3. ANALYSIS OF Na I AND Ca II DATA

A synthetic summary of the different interstellar components detected in Ca II and Na I toward the stars of our sample is presented in Table 4. For each component we list the heliocentric radial velocity, V_{HEL} (km s^{-1}), the equivalent width, W_λ (mÅ), and the column density, N (atoms cm^{-2}). For a few stars of our sample, Ca II spectra were not available, and were integrated with data taken from LVF. Errors in the equivalent widths are generally lower than about 1 mÅ. The internal accuracy in radial velocity, resulting from the wavelength calibration of our spectra, is about 0.2 and 0.1 km s^{-1} for the Ca II and Na I regions, respectively. The uncertainties in the Na I and Ca II column densities range from about $\pm$0.02 dex for the best cases to about $\pm$0.15 dex for the weakest features. The lines fall on the linear part of the curve of growth, with the sole exception of Na I in HD 129685, which shows some saturation, and for which we have been able to derive the microturbulence parameter, $b = 1.2\,(\pm 0.2)$ km s^{-1}. This accurate determination of the line-of-sight velocity dispersion makes it possible to derive a stringent upper limit on the kinetic temperature of the gas, $T < 2.7 \times 10^3$ K, by assuming that all the broadening is due to thermal motions rather than to turbulence.

3.1. *Radial Velocity Analysis*

In order to identify the absorption detected in our spectra, we searched for velocity coincidences between our radial velocities and the line-of-sight projected velocities of nearby inter-

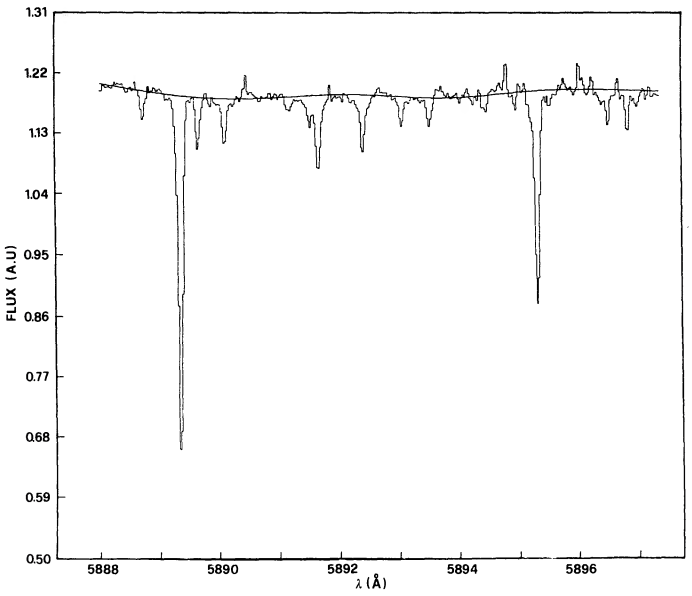

FIG. 2a

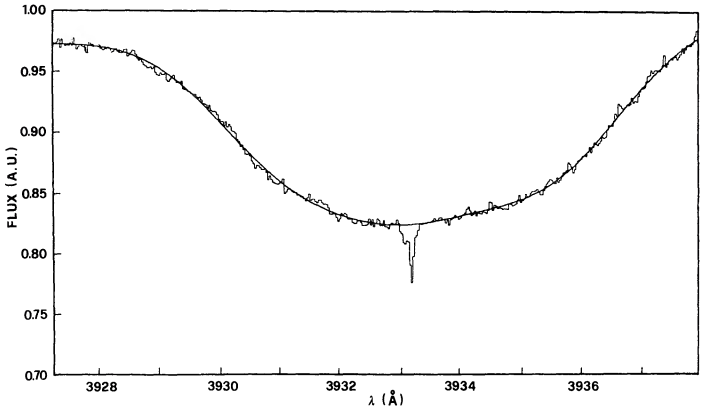

FIG. 2b

FIG. 2.—Examples of continuum tracing. (*a*) Na I region for HD 129685; this spectral range is heavily contaminated by telluric absorptions. (*b*) Ca II K region for the same star.

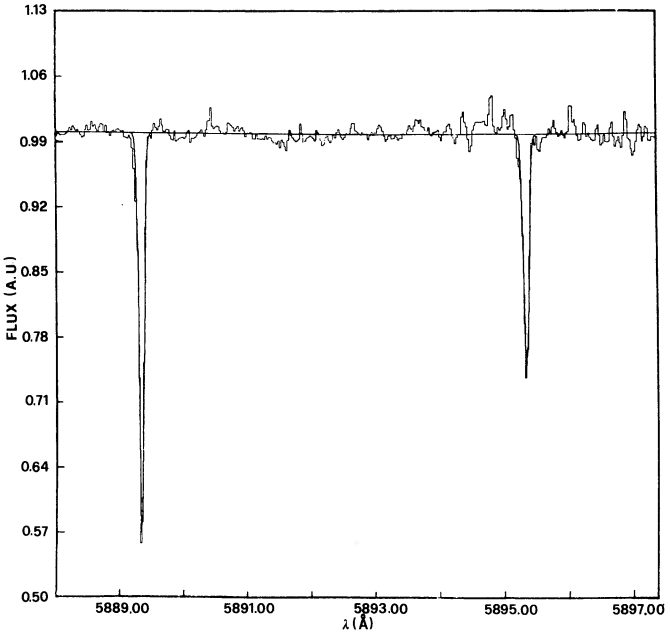

FIG. 3a

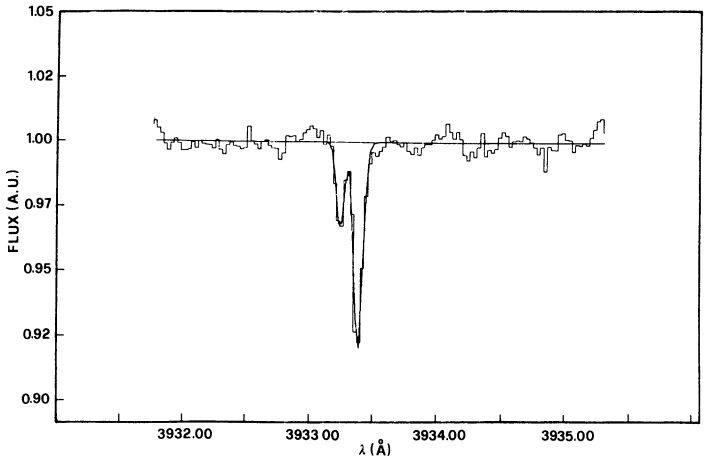

FIG. 3b

FIG. 3.—Examples of normalized spectra. (*a*) Na I interstellar spectrum toward HD 129685 after correction for telluric absorptions. (*b*) Ca II K interstellar spectrum toward HD 119921; the weaker absorption is produced by the component *P* of Lallement, Vidal-Madjar, & Ferlet (1986); the stronger one by gas moving according to Crutcher's (1982) velocity.

TABLE 4

Ca II AND Na I INTERSTELLAR ABSORPTIONS TOWARD THE STARS OF TABLE 1

	Ca II				Na I					
STAR	V_{HEL} km s^{-1}	W_K mÅ	W_H mÅ	log N cm^{-2}	V_{HEL} km s^{-1}	W_{D2} mÅ	W_{D1} mÅ	log N cm^{-2}	COMPONENT	Na I/Ca II
ι Cen	−17.7[a]	2.3[a]	...	10.38[a]	...	<2.5	<2.5	<10.10	*P*	<0.52
HD 119921	−21.5	2.6	1.9	10.44	...	<0.8	<0.8	<9.60	*P*	<0.14
	−10.0	7.1	5.7[b]	10.87	−8.8	36.6[c]	17.3	11.25	*AI C*	2.41
ζ Cen	−12.6	4.3	0.9[b]	10.66	−12.0	5.9[c]	2.7	10.48	*I BC*	0.64
	−2.8	1.1	<0.7	10.07	...	<0.6	<0.6	<9.50	*U*	<0.26
φ Cen	−15.6	4.0	[d]	10.64	−13.8[b]	8.7[b]	3.6	10.67	*BC*	1.02
	−8.2	3.4	[d]	10.60	−8.5	13.2[c]	8.0	10.82	*A C*	1.82
	−1.7	2.0	[d]	10.30	−2.0[b]	2.7[c]	0.9[b]	10.10[b]	*U*	0.63[b]
ψ Cen	...	...	...	...	−31.3	2.1	<1.3	10.02	*U*	...
	...	...	...	...	−21.5	4.8[c]	3.1	10.38	*P*[e]	...
	...	...	...	...	−10.7	4.1	<1.3	10.31	*A C*	...
η Cen	...	<0.5	<0.6	<9.70	−23.0	1.0[b]	1.3[b]	9.70	*P*	>0.94
	...	<0.5	<0.6	<9.70	−12.4	4.7	4.2[b]	10.38	*O CB*	>4.40
HD 129685	−26.3	2.0	0.6[b]	10.40	...	<1.4	<1.4	<9.80	*P*	<0.33
	−16.9	4.4	2.7	10.67	−16.2	41.4	26.2	11.53[f]	*BC*	6.5
α Vir	−11.1[a]	2.6[a]	...	10.4[a]	−11.3	9.0[c]	3.7	10.65	*O BC*	1.62
	−3.2	2.6[a]	...	10.4[a]	...	<0.8	<0.8	<9.60	*I*	<0.14

[a] Data from Lallement, Vidal-Madjar, & Ferlet 1986.
[b] Uncertain due to noise or possible stellar contamination.
[c] Telluric line eliminated using a template spectrum.
[d] Strong photospheric absorption.
[e] Coincidence at −1.8 km s^{-1} with Panoramix component.
[f] Microturbulence parameter from the doublet ratio method $b = 1.15$ km s^{-1}.

stellar clouds. The comparison was made with the motion of the gas flowing inside the solar system derived from backscattering measurements (Bertaux 1984), with the four clouds identified by LVF, and with the global flow of the LISM within $\simeq 100$ pc (Crutcher 1982). The results are displayed in the penultimate column of Table 4. A coincidence within ± 1 km s^{-1} with one of the radial velocities predicted by LVF is indicated with the name of the cloud given by these authors: *P* (Panoramix), *I* (Idefix), *O* (Obelix) and *A* (Asterix). The quality of our data is sufficient to allow detection of the weak components reported by LVF. In fact, about 70% of the Ca II column density values reported by LVF are higher than our detection limit ($\log N_{\rm Ca\,II} \simeq 10.0$). A coincidence within ± 3 km s^{-1} with the projected velocities predicted by Bertaux (1984) or Crutcher (1982) is indicated with the letter *B* or *C*, respectively. The velocity intervals adopted for the coincidence analysis were chosen on the basis of the uncertainties quoted by the authors.

3.1.1. *The Very Local ISM*

The gas entering the solar system and moving with the velocity vector given by Bertaux (1984) is characterized by a space density of hydrogen atoms $n_{\rm H\,I} \approx 0.1$ cm^{-3}. If such gas is due to a local cloud surrounding the Sun and extended by about $d \approx 3$ pc, we expect a hydrogen column density $N_{\rm H\,I} \approx 10^{18}$ cm^{-2} and therefore a Na I column density $N_{\rm Na\,I} \simeq 10^{9}$ cm^{-2}, when we use the correlation between $N_{\rm H\,I}$ and $N_{\rm Na\,I}$ given by Ferlet, Vidal-Madjar, & Gry (1985). In our Na I spectra, the absorptions at *B* velocity show Na I column densities which exceed, by at least a factor 25, this value of $N_{\rm Na\,I}$. Therefore we believe that these absorptions share the *B* velocity just by chance. In the Ca II spectra of LVF, the Bertaux (1984) motion is detected without ambiguity only toward a few stars in the Galactic longitude range $60° \leq l \leq 180°$, i.e., quite far from our area.

3.1.2. *The Panoramix Component*

According to LVF this component is present at less than 5 pc from the Sun and covers approximately the region of the sky within the Galactic longitude range $300° \leq l \leq 60°$ and Galactic latitude range $-60° \leq b \leq 40°$. All the stars shown in Figure 1 fall within this range and are located beyond 5 pc. From Table 4 one can see that there are five detections, mainly in Ca II, out of the seven stars investigated in the optical. Our results confirm the presence of the cloud and, at the same time, indicate that it is very patchy. In fact, we find variations in $N_{\rm Na\,I}$ up to a factor of 6 on angular scales of 6°. If the cloud is at a distance $d \simeq 5$ pc from the Sun, these angular variations correspond to spatial variations on a distance scale of $\simeq 0.5$ pc within the cloud.

3.1.3. *The Idefix Component*

All our stars are located within the region of the sky proposed by LVF for this component, but absorptions at *I* velociy are not found for the majority of them. The lack of detection in the two stars of the sample of LVF closest to our targets (ι Cen, α Lup), indicates that the component *I* must be tenuous in our field. The only stars of Figure 1 with absorption features sharing *I* velocity are HD 119921 and ζ Cen. In the direction of HD 119921, the Ca II absorption is higher by a factor of 3 than the strongest Ca II feature found by LVF at *I* velocity, and the Na I/Ca II ratio is greater than 1, in contrast with the Na I/Ca II ratio found for this component toward α Vir (§ 3.2). This suggests that the bulk of the absorption in front of HD 119921 is associated with a different cloud that, by chance, has the same velocity as Idefix. In the direction of ζ Cen, the Na I/Ca II ratio is less than 1, and this star is the only potential candidate for the detection of the component *I* among our targets.

3.1.4. *The Asterix Component*

According to LVF this component covers a large part of the sky and is located within $\simeq 5$ pc of the Sun. Three stars angularly close in our field show an absorption sharing the *A* projected velocity: HD 119921, ϕ Cen and ψ Cen. The Na I/Ca II ratios in HD 119921 and ϕ Cen (Na I/Ca II $\simeq 2$), are higher by one order of magnitude than the one found toward α Oph for the component *A* (§ 3.2). Therefore, either this component shows remarkable variations in the Na I/Ca II ratio, or the absorptions in HD 119921, ϕ Cen and ψ Cen are produced elsewhere. Since the radial velocities of these features in our stars also show a coincidence with Crutcher's flow, they may well be produced in more distant gas, sharing by chance the *A* projected velocity.

3.1.5. *The Obelix Component*

This component is not seen in six out of the seven stars of our sample. Only in η Cen do we find an absorption feature whose radial velocity is in agreement with the *O* velocity vector. The absorption feature is also in agreement with Crutcher's flow and may be produced by more distant gas (η Cen is at 130 pc). The two stars in the LVF sample angularly closest to our targets (ι Cen and α Lup) do not show absorption features at *O* velocity.

3.1.6. *Crutcher's Flow*

The strongest absorption components in our stars show a velocity coincidence within ± 3 km s^{-1} with Crutcher's flow. According to LVF, Crutcher's flow is a sort of average of the motions of nearby clouds. Our data show that not all the absorptions sharing Crutcher's velocity can be associated with local clouds. For instance, the strongest absorption in HD 129685, which is in agreement both with Bertaux and with Crutcher vectors, is not likely to be produced by the local gas entering the solar system, on the basis of our previous discussion (3.1.1). Therefore we associate this absorption with more distant gas, moving according to Crutcher's flow. Similar conclusions can be applied to the -12 km s^{-1} component in η Cen and to the -14 km s^{-1} component in ϕ Cen. In these cases one would expect to find some absorptions produced by nonlocal gas, owing to the larger distances to these targets (130 pc and 213 pc, respectively).

3.1.7. *Unidentified Components*

In three lines of sight (ζ Cen, ϕ Cen and ψ Cen) we find an absorption component whose radial velocity cannot be identified with any of the LISM motions above discussed. Toward the angularly close pair of stars ζ Cen and ϕ Cen, the radial velocities of the unidentified features are quite similar ($\simeq -2$ km s^{-1}), as are the Na I/Ca II ratios (smaller than 1). If we associate these two absorptions with a single cloud located at a distance *d*, the angular separation of the two stars indicates that the cloud must be extended at least 8.7 (d/100) pc.

3.2. Na I/Ca II *Ratios*

It is well-known that the Na I/Ca II ratio is of the order of unity, or greater, for low-velocity interstellar clouds and drops off rapidly when $|V_{\rm LSR}| \geq 10$–20 km s^{-1} (Routly & Spitzer 1952; Siluk & Silk 1974). According to the most common interpretation of the Routly-Spitzer effect, the variations of the

Na I/Ca II ratio are predominantly an abundance effect, mainly due to variation of the calcium abundance, rather than an ionization effect (Hobbs 1983). The variation of the abundance is induced by grain disruption in shocked gas, and this explains why the Ca II abundance increases (i.e., the ratio decreases) in high-velocity gas.

In the last column of Table 4 we list the observed Na I/Ca II ratio for our components. For the *P*-component the upper limits are less than 1, in agreement with the relatively high velocity of the observed absorptions. For the *I*-component we have derived the Na I/Ca II ratio in the direction of α Vir, combining our Na I upper limit with the Ca II data of LVF. The resulting ratio, Na I/Ca II < 0.14, can be explained in terms of the Routly-Spitzer effect, if one considers the modulus of the *I* velocity vector given by LVF, $V_{LSR} = 26$ km s^{-1}, instead of the projected velocity along the line of sight which is quite low. The Na I/Ca II ratio for the component *A* can be estimated in the direction of α Oph ($l = 36°$, $b = +23°$, $r = 17$ pc), which shows a single Ca II absorption at the *A* velocity (LVF). By using the data listed by Frisch (1981), we find also for the component *A* a value characteristic of high-velocity gas (Na I/Ca II $\simeq 0.2$). In this case the modulus of the velocity vector found by LVF is relatively small ($V_{LSR} = 11$ km s^{-1}).

In summary, the local interstellar clouds ($d \leq 20$ pc) are characterized by Na I/Ca II ratios less than 1. This can be the result of grain disruption within tenuous clouds embedded in the Local Bubble owing to the passage of a shock front. According to Frisch (1981), the low velocity of the observed absorptions toward α Oph can be explained in terms of a supernova remnant which has slowed down since the passage of the shock front.

Also the unidentified absorptions observed toward ζ Cen and ϕ Cen have Na I/Ca II < 1. Given the distances to these stars, these unidentified components may be produced in clumps of shocked gas located either in the Local Bubble or within the nearby Loop I Bubble (§ 4.1).

The situation is different for the most intense components of our spectra which have Na I/Ca II ratios greater than 1, including a quite large value in the direction of HD 129685 (Na I/Ca II = 6.5). The radial velocities of these absorptions are in agreement with the projection of Crutcher's velocity vector. The high Na I/Ca II values suggest a low efficiency of the grain disruption processes during the acceleration of these layers of gas up to the velocity of Crutcher's flow.

3.3. *Number of Components Along the Line of Sight*

The multiple-component structure detected in Ca II and Na I can be used to estimate the average intercloud distance along the line of sight, $\lambda = r/n_c$, where n_c is the number of components detected in a given line of sight of length r. In Figure 4 we show λ as a function of r for our stars. One can see that λ is higher at larger distances, a fact which suggests a cloud deficiency beyond a certain distance. For the sake of comparison, in the same figure we show the typical intercloud distance predicted by the McKee & Ostriker (1977) model for the warm envelopes of interstellar clouds, $\lambda_w \simeq 12$ pc. One can see that λ is in general higher than λ_w, the departures from the predicted value becoming significant beyond about 70 pc. The lack of detection of new interstellar components, in spite of the high S/N ratio of our optical spectra, is consistent with the three-dimensional distribution of the gas discussed in § 4.2.

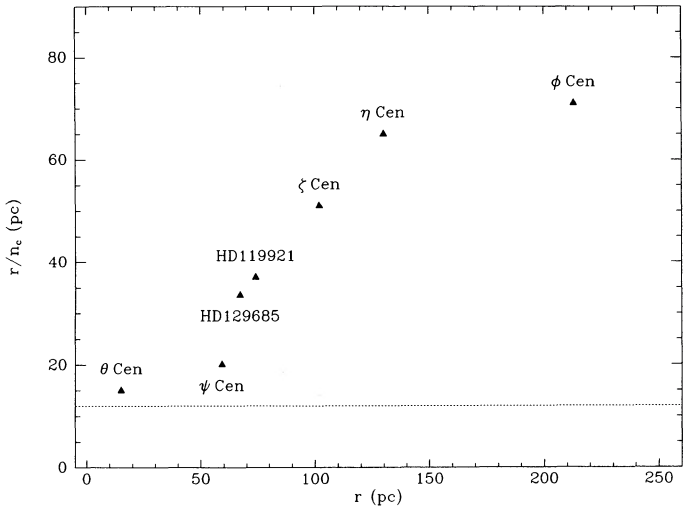

FIG. 4.—The average intercloud distance, $\lambda = r/n_c$, as a function of the distance to our stars. The dashed line represents the predicted intercloud distance between the warm envelopes of interstellar clouds, according to the model of McKee & Ostriker (1977).

4. ANALYSIS OF THE ULTRAVIOLET DATA

4.1. *Equivalent Widths and Column Densities*

In Table 5 we list the equivalent widths of interstellar lines measured in our *IUE* spectra. Laboratory wavelengths and oscillator strengths, *f*, are from Morton & Smith (1973), except where indicated. When more than one spectrum was available for a given line of sight, we measured W_λ from the best exposed spectrum in the spectral range of interest. The multiple component structure observed in Ca II and Na I is not resolved at the spectral resolution of the *IUE* spectra (FWHM $\simeq 20$ km s^{-1}). The data for ψ Cen and ϕ Cen are not listed in Table 5 because the optical spectra of these two stars show two or even three components of comparable intensity which fall within one *IUE* instrumental profile. Also ι Cen is excluded from the table, because its relatively low rotational velocity prevented us from disentangling interstellar lines from stellar features. All the other lines of sight show a prominent absorption in the optical, sharing Crutcher's velocity, plus a weaker absorption, generally associated with the *P* component of LVF. We assume that the UV absorptions in these lines of sight (HD 119921, ζ Cen, η Cen and HD 129685) are essentially due to the strongest Crutcher component, with a negligible contribution from the nearby weaker component. An inspection of the high-resolution UV profiles of ζ Cen and η Cen obtained by means of the *Copernicus* satellite (Wisconsin Astrophysics, n. 156) confirms the presence of a single component along these two lines of sight.

In Table 6 we give the column densities, N (atoms cm^{-2}), and microturbulence parameters, b (km s^{-1}), for the UV species. Mg II column densities are not considered, owing to the large degree of saturation of the Mg II doublet. For the singly ionized species the *b*-values were obtained from the best fits of Fe II, Si II and S II, and adopted for Zn II. The uncertainty on the *b*-value does not affect severely the Zn II column densities, given the low degree of saturation (if any) of the Zn II doublet. For Mg I we estimated the *b*-values indirectly from those derived from the line broadening of Na I and Ca II lines. An uncertainty of ± 1 km s^{-1} in these *b*-values was adopted

TABLE 5

INTERSTELLAR LINES IN THE ULTRAVIOLET RANGE

Ion	λ	f_λ	References	HD 119921 W_λ	ζ Cen W_λ	η Cen W_λ	HD 129685 W_λ
Mg I	2025.824	0.110	1	<11	<13	<13	<15
	2852.127	1.77	1	53 $(^{+18}_{-22})$	33 $(^{+11}_{-16})$	49 ($\pm$17)	64 $(^{+12}_{-15})$
Mg II	2795.528	0.592		371 ($\pm$19)	289 ($\pm$15)	267 ($\pm$14)	305 ($\pm$21)
	2802.704	0.295		304 $(^{+18}_{-16})$	289 ($\pm$17)	246 ($\pm$13)	210 ($\pm$16)
Si II	1260.421	1.16	2	BS	172 ($\pm$33)	156 ($\pm$10)	BS
	1304.372	0.10	2	BS	93 ($\pm$18)	103 ($\pm$18)	<129
	1526.708	0.116	2	131 ($\pm$20)	127 ($\pm$20)	117 ($\pm$15)	103 ($\pm$16)
	1808.012	0.0041	2	42 ($\pm$9)	20 ($\pm$14)	30 ($\pm$10)	30 ($\pm$10)
S II	1250.586	0.00535		<46	44 ($\pm$12)	63 ($\pm$8)	BS
	1253.812	0.0107		45 ($\pm$11)	60 ($\pm$14)	72 ($\pm$12)	BS
	1259.520	0.0159		62 ($\pm$25)	62 ($\pm$9)	94 ($\pm$9)	BS
Fe II	1608.451	0.062	3	73 ($\pm$18)	49 ($\pm$10)	65 ($\pm$16)	71 ($\pm$12)
	2343.496	0.108	3	139 ($\pm$37)	150 ($\pm$45)	111 ($\pm$22)	147 ($\pm$25)
	2373.736	0.0395	3	111 ($\pm$42)	80 ($\pm$27)	<95	92 ($\pm$20)
	2382.038	0.328	3	200 ($\pm$31)	208 ($\pm$28)	149 ($\pm$26)	153 ($\pm$29)
	2585.876	0.0573	3	170 ($\pm$33)	123 ($\pm$25)	91 ($\pm$30)	148 ($\pm$17)
	2599.396	0.203	3	220 ($\pm$24)	181 ($\pm$13)	174 ($\pm$23)	159 ($\pm$23)
Zn II	2025.512	0.412		46 ($\pm$8)	32 ($\pm$6)	25 ($\pm$7)	36 ($\pm$8)
	2062.016	0.202		25 $(^{+10}_{-7})$	<18	*S*	16 $(^{+10}_{-11})$

NOTES.—BS: Bad subtraction of the background in the *IUE* image. *S*: Strong photospheric absorption.
REFERENCES.—(1) Morton 1978; (2) de Boer, Jura, & Shull 1987; (3) Shull, Van Steenberg, & Seab 1983.

and propagated in the error analysis of the Mg I column densities.

4.2 *Depth Distribution of the Gas*

In Figure 5 we plot the H I column densities as a function of the distance to the background star, *r*, in the field under investigation (*filled symbols*). The H I column densities are not available for our targets, with the sole exception of η Cen ($N_{\rm H\,I}$ = 20.11; Bohlin et al. 1983), and were derived indirectly from the column densities of other ions. For θ Cen we converted $N_{\rm Mg\,II}$ (Genova et al. 1990) into $N_{\rm H\,I}$ by using a magnesium depletion of -0.4 dex (Murray et al. 1984). For our targets we converted $N_{\rm Zn\,II}$ into $N_{\rm H\,I}$ by means of the relation given by Harris & Mas Hesse (1986). In the case of ϕ Cen we derived $N_{\rm Zn\,II}$ from the equivalent width of the Zn II unsaturated absorption at 2062 Å, $W_\lambda = 26(\pm 10)$ mÅ. For the sake of comparison we include also μ Cen ($l = 314°$, $b = +19°$, $r = 120$ pc) which has a direct $N_{\rm H\,I}$ measurement (Bohlin et al. 1983).

In spite of the uncertainties inherent in the conversions to $N_{\rm H\,I}$, two facts are clear from Figure 5: a strong increase in $N_{\rm H\,I}$ between 15 and 65 pc, and an approximately constant value at larger distances. These facts can be explained well in terms of the schematic representation of the Local Bubble and of the Loop I Bubble sketched by Iwan (1980) and by Cox & Reynolds (1987). According to this scenario, a wall of neutral gas separates the Local Bubble from Loop I Bubble, the nearest side being in the direction $l \simeq 330°$ and $b \simeq 20°$. The stars in front of the wall should be located within the Local Bubble and should show a low interstellar absorption (log $N_{\rm H\,I} \leq 18$). This seems to be the case of θ Cen. The stars beyond the wall should present an increase in $N_{\rm H\,I}$, followed by an approximately constant value due to the fact that the lines of sight are entering the Loop I Bubble. Our results confirm the validity of this scenario, and provide stringent limits ($d = 40 \pm 25$ pc) to the distance to the nearest side of the wall in the field $310° \leq l \leq 330°$ and $15° \leq b \leq 25°$. This distance is about one-half of that suggested by Iwan (1980), but very close to that presented by Cox & Reynolds (1987). This kind of result is important for testing models which reproduce the soft X-ray emission background in terms of thermal emission from nearby gas (Snowden et al. 1990).

As it was already noted by Iwan (1980), the wall of neutral gas has a column density $N_{\rm H\,I} \approx 10^{21}$ cm^{-2} in the region of Galactic coordinates $330° \leq l \leq 30°$ and $0° \leq b \leq 40°$ adjacent to our field. In Figure 5 we plot the published $N_{\rm H\,I}$ values in this longitude range (*empty symbols*), confining our attention to the same strip of latitudes of our field ($15° \leq b \leq 25°$). One can see that for these lines of sight there is an increase of $N_{\rm H\,I}$ by

TABLE 6

LOGARITHMIC COLUMN DENSITIES AND *b*-VALUES FROM THE ULTRAVIOLET DATA

	HD 119921		ζ Cen		η Cen		HD 129685	
COLUMN	log *N*	*b*	log *N*	*b*	log *N*	*b*	log *N*	*b*
Si II	$14.65^{+0.03}_{-0.04}$	7.2	$14.25^{+0.03}_{-0.03}$	9.0	$14.46^{+0.20}_{-0.17}$	7.8	$14.49^{+0.04}_{-0.03}$	5.8
S II	$14.68^{+0.05}_{-0.04}$	7.2	$15.06^{+0.24}_{-0.11}$	5.0	$15.23^{+0.26}_{-0.09}$	6.6	...	...
Fe II	$13.99^{+0.14}_{-0.07}$	7.2	$13.72^{+0.07}_{-0.10}$	7.8	$13.88^{+0.13}_{-0.12}$	5.2	$14.08^{+0.32}_{-0.10}$	5.4
Zn II	$12.57^{+0.10}_{-0.08}$	...	$12.41^{+0.01}_{-0.08}$	...	$12.27^{+0.11}_{-0.13}$	...	$12.42^{+0.08}_{-0.07}$	...
Mg I	$11.91^{+0.49}_{-0.11}$	2.6	$11.51^{+0.02}_{-0.05}$	3.6	$11.71^{+0.06}_{-0.03}$	4.3	$12.42^{+0.38}_{-0.41}$	2.0

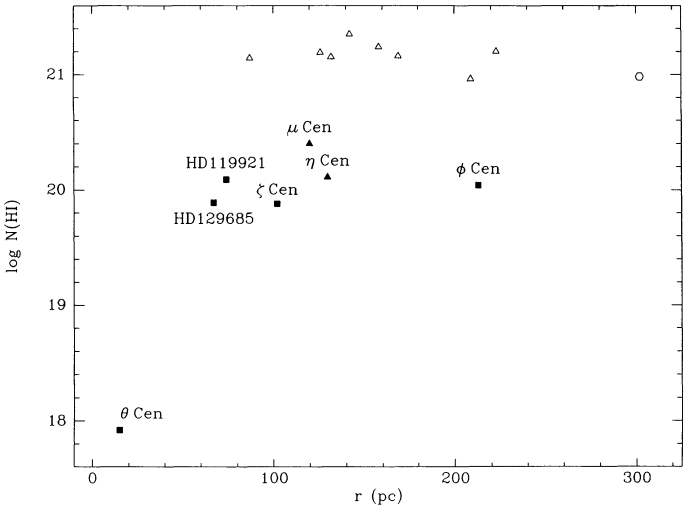

FIG. 5.—Distribution of interstellar H I column densities as a function of distance in the strip of Galactic latitudes $15 \leq b \leq 25$ toward the center of Loop I. *Filled symbols:* stars within the Galactic longitude range $310 \leq l \leq 330$ investigated in this work. *Empty symbols:* stars within the adjacent longitude range $330 \leq l \leq 30$. *Squares:* our data (see text). *Filled triangles:* data from Bohlin et al. (1983). *Empty triangles:* data from Bohlin, Savage, & Drake (1978). *Hexagon:* data from Shull & Van Steenberg (1985). For the sake of homogeneity, the distances to all the stars have been computed by adopting the criteria mentioned in § 2.

almost one order of magnitude higher than in our field. The distance to the nearest side of the wall is within $\simeq 90$ pc in this field.

On the basis of the above discussed three-dimensional distribution, it is clear that the strong absorptions observed at Crutcher's velocity in our optical spectra must be produced by the gas located between the Local Bubble and Loop I Bubble. This confirms our suggestion, advanced in § 3.2, that the bulk of the absorptions observed in HD 119921, ϕ Cen and ψ Cen are not produced by the nearby ($d \leq 5$ pc) component *A* of LVF. It is also unlikely that the absorption seen in ζ Cen is produced in the nearby ($d \leq 20$ pc) component *I*.

5. PHYSICAL STATE OF THE GAS

Ratios of interstellar atoms/ions involving trace species, such as Na I and Mg I, are very sensitive to the physical state of the absorbing clouds. In Table 7 we show the values of some ratios, obtained by combining optical and UV column densities under the assumption that each of the four lines of sight considered here intercepts essentially a single interstellar component (§ 4). One can see that the ratios are higher in ζ Cen and η Cen than in the other two lines of sight, and this is clear in particular for the Zn II/Na I ratio. We interpret the differences in the Zn II/Na I ratios as due to an ionization effect rather than to an abundance effect. In fact, zinc and sodium depletions are quite constant in the interstellar space (Harris & Mas Hesse 1986; Phillips, Pettini, & Gondhalekar 1984). Also, since Zn II is the dominant ionization state of zinc, we interpret the differences in the Zn II/Na I ratios as due to variations of the sodium ionization balance, possibly induced by temperature variations. This qualitative conclusion will be confirmed in the following paragraphs, where we compare in a quantitative way the observed Mg I/Na I and Zn II/Mg I ratios with the theoretical ones.

TABLE 7

IONIZATION RATIOS

HD	Name	Zn II/Na I	Mg I/Na I	Zn II/Mg I
119921.....	...	21 ($^{+6}_{-4}$)	4.6 ($^{+1.3}_{-3.1}$)	4.6 ($^{+2.8}_{-3.4}$)
121263.....	ζ Cen	85 ($^{+10}_{-16}$)	10.7 (± 1.0)	7.9 ($^{+1.2}_{-1.6}$)
127972.....	η Cen	78 ($^{+27}_{-23}$)	21.4 (± 4.0)	3.6 ($^{+1.4}_{-1.3}$)
129685.....	...	7.8 ($^{+1.7}_{-1.3}$)	7.8 ($^{+11}_{-5}$)	1.0 ($^{+2.1}_{-0.6}$)

5.1 *The Temperature*

Under the basic assumption of ionization equilibrium, Pettini et al. (1977) showed that the Mg I/Na I ratio is quite sensitive to the temperature, T, and that it is almost independent of the electron density, n_e, and of the interstellar radiation field. The ratio is quite constant for $T \leq 7 \times 10^3$ K and increases rapidly at higher temperatures. We have computed the theoretical ratio Mg I/Na I as a function of T by adopting an updated set of input parameters with respect to those used by Pettini et al. (1977). A similar computation was performed by Keenan, Bates, & Catney (1986), without including the effect of collisional ionization. From the condition of ionization equilibrium for the element X, one has (see Pottasch 1972)

$$\frac{n_{X^+}}{n_{X^0}} = \frac{\Gamma_{X^0} + C_{X^0}(T) n_0}{\alpha_{X^+}(T) n_e}, \quad (1)$$

where Γ_{X^0} is the photoionization rate (s^{-1}), $C_{X^0}(T)$ is the collisional ionization coefficient ($cm^3\ s^{-1}$), and $\alpha_{X^+}(T)$ is the total recombination coefficient ($cm^3\ s^{-1}$). For the elements with first ionization potential less than 13.6 eV, such as Na and Mg, the dominant ionization state, even in H I regions, is the singly ionized one due to photoionization of the neutral species in the energy range below the hydrogen ionization threshold. Therefore one can assume $n_{Mg} \simeq n_{Mg\ II}$ and $n_{Na} \simeq n_{Na\ II}$. From these assumptions, and by applying equation (1) to Mg and Na, one can derive the following expression:

$$\frac{n_{Mg\ I}}{n_{Na\ I}} = \left[\frac{Mg}{Na}\right]_{cosmic} \times 10^{\delta_{Mg} - \delta_{Na}} \left[\frac{\alpha_{Mg\ II}(T)}{\alpha_{Na\ II}(T)}\right] \left[\frac{\Gamma_{Na\ I} + C_{Na\ I}(T) n_e}{\Gamma_{Mg\ I} + C_{Mg\ I}(T) n_e}\right], \quad (2)$$

where $\delta_X = \log [N_X/N_H] - \log [X/H]_{cosmic}$ is the depletion of the element X, and $[X/H]_{cosmic}$ is its cosmic abundance. If one assumes that the ratio of the volume densities $n(X)$ may be equated to the ratio of the column densities $N(X)$, i.e., that the different species have the same distribution along the line of sight, one can use equation (2) to compute the theoretical Mg I/Na I ratio. The results are shown in Figure 6, for the case of equal depletion of Na and Mg. The Mg^0 and Na^0 photoionization rates are taken from Keenan (1984), while the collision ionization coefficients are from Arnaud & Rothenflug (1985). The recombination coefficients for Mg^0 and Na^0 are taken from Shull & Van Steenberg (1982) and from the computer code of Arnaud & Rothenflug (1985), respectively. On the basis of the results of Jacobs (1985), we neglect the dielectronic recombination for Na^+ at low temperatures ($T \leq 25 \times 10^3$ K). By comparing the charge-exchange rates quoted by Péquignot & Aldrovandi (1986) with the typical values of the ionization and recombination rates in equation (1), we have checked that charge exchange reactions involving magnesium and sodium can be neglected.

The dependence of the Mg I/Na I ratio on the depletion is quite critical. In particular, while sodium depletion is quite constant in the interstellar gas (Phillips et al. 1984), magnesium

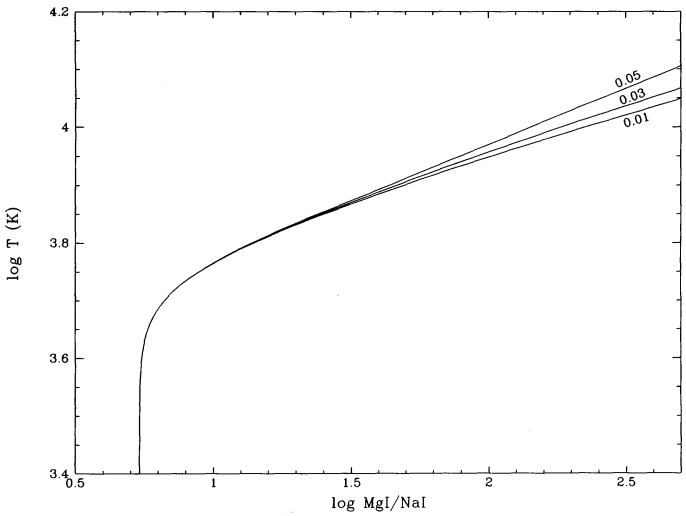

FIG. 6.—Theoretical Mg I/Na I ratio as a function of temperature in the case of equal depletion for magnesium and sodium. Cosmic abundances are taken from Grevesse (1984). The different curves correspond to different values of the electron density, indicated in units of cm^{-3}.

depletion shows a range of values which span from almost absence of depletion up to about -1.0 dex (Murray et al. 1984). For our lines of sight we find $\delta_{Mg} = -0.76$ dex for η Cen and $\delta_{Mg} = -0.63$ dex for ζ Cen. For the first star we have estimated directly δ_{Mg} from the data listed by Murray et al. (1984). In the case of ζ Cen we have first computed $N_{H\,I}$ as explained in § 4.2, and then $N_{Mg\,II}$ from the equivalent width of the Mg II line at 1240 Å (Bohlin et al. 1983), adopting the same oscillator strength used by Murray et al. (1984). In both lines of sight the magnesium depletion is very close to the average of the sodium depletions found by Phillips et al. (1984), $\delta_{Na} \simeq -0.7$ dex. We assume that also along the other two lines of sight (HD 119921 and HD 129685) sodium and magnesium have equal depletions.

In Table 8 we list the temperatures, $T_{Mg\,I/Na\,I}$, derived from the comparison of the observed Mg I/Na I ratios with the theoretical curve shown in Figure 6. The errors ϵ_T have been computed by considering the maximum range of $T_{Mg\,I/Na\,I}$ values allowed by (i) an uncertainty of ± 0.2 dex in the depletions term $\delta_{Mg} - \delta_{Na}$, and (ii) the errors on the observed ratios listed in Table 7. We find evidence of warm gas in front of ζ Cen ($T \simeq 6 \times 10^3$ K) and η Cen ($T \simeq 7 \times 10^3$ K), and of slightly colder gas toward the other two stars. In the direction of HD 129685 we derive a more stringent upper limit on the temperature, $T < 2.7 \times 10^3$ K, from the line-of-sight velocity dispersion of Na I lines (§ 3). The comparison between HD 129685 (Zn II/Na I $\simeq 8$; $T < 2.7 \times 10^3$ K) and ζ Cen or η Cen (Zn II/Na I $\simeq 80$; $T \simeq 6$–7×10^3 K), together with our qualitative discussion at the beginning of § 5, suggest that the Zn II/Na I ratio is quite sensitive to the temperature. If this is true, the relatively low Zn II/Na I ratio found in HD 119921 gives an independent indication that the gas along this line of sight is colder than that toward ζ Cen or η Cen.

TABLE 8

PHYSICAL PARAMETERS

HD	Name	$T_{Mg\,I/Na\,I}$ ($\times 10^3$ K)	ϵ_T ($\times 10^3$ K)	n_e (cm^{-3})	ϵ_{n_e} (cm^{-3})	$\bar{n}_{H\,I}$ (cm^{-3})
119921.....	...	4.6	$^{+1.1}_{-4.6}$	...	...	0.55
121263.....	ζ Cen	6.0	$^{+0.7}_{-1.1}$	0.039	$^{+0.023}_{-0.016}$	0.25
127972.....	η Cen	6.9	$^{+0.8}_{-1.0}$	0.029	$^{+0.028}_{-0.015}$	0.33
129685.....	...	5.4	$^{+1.9}_{-5.4}$	...	...	0.39

5.2. *The Electron Density*

In order to cast more light on the physical state of the absorbing gas, we have investigated the behavior of the Zn II/Mg I ratio as a function of the temperature and electron density. From the condition of ionization equilibrium (1) for magnesium, and by assuming $n_{Zn} \simeq n_{Zn\,II}$ and $n_{Mg} \simeq n_{Mg\,II}$, it is easy to derive the following expression:

$$\frac{n_{Zn\,II}}{n_{Mg\,I}} \simeq \left[\frac{Zn}{Mg}\right]_{cosmic} \times 10^{\delta_{Zn} - \delta_{Mg}} \left[\frac{\Gamma_{Mg\,I} + C_{Mg\,I}(T) n_e}{\alpha_{Mg\,II}(T) n_e}\right]. \quad (3)$$

From this equation one can express the electron density as follows:

$$n_e \simeq \Gamma_{Mg\,I} \Big/ \left[\alpha_{Mg\,II}(T) \frac{n_{Zn\,II}}{n_{Mg\,I}} \left[\frac{Mg}{Zn}\right]_{gas} - C_{Mg\,I}(T)\right], \quad (4)$$

where $[Mg/Zn]_{gas} = [Mg/Zn]_{cosmic} \times 10^{\delta_{Mg} - \delta_{Zn}}$. In Table 8 we list the electron densities derived from equation (4) by assuming that the ratio of the volume densities, $n_{Zn\,II}/n_{Mg\,I}$, can be equated to the ratio of the column densities, Zn II/Mg I. We have considered only the lines of sight of ζ Cen and η Cen, for which we were able to significantly constrain the temperature from the analysis of the Mg I/Na I ratio. The same ionization and recombination rates used for the analysis of the Mg I/Na I ratio have been adopted. The collision ionization and total recombination rates have been computed at the temperature corresponding to each line of sight. As far as the depletions are concerned, we derived $\delta_{Zn} \simeq -0.1$ dex fo ζ Cen, and $\delta_{Zn} \simeq -0.4$ dex for η Cen from our Zn II column densities. The adopted magnesium depletions are quoted in § 5.1. The errors on the electron densities listed in Table 8, ϵ_{n_e}, have been derived by taking into account (i) the error on the observed Zn II/Mg I ratio shown in Table 7, (ii) the temperature error ϵ_T, and (iii) an uncertainty of ± 0.1 dex on the depletions. The effect of each source of error has been computed separately, and the partial errors have been added up in quadrature to derive ϵ_{n_e}.

It must be noted that the resulting electron densities scale linearly with the photoionization rate—as can be seen from equation (4)— and could be therefore increased (or decreased) if the local radiation field within the absorbing gas were more (or less) intense than that given by Gondhalekar, Phillips, & Wilson (1980), and adopted by Keenan (1984) in his derivation of $\Gamma_{Mg\,I}$.

In the last column of Table 8 we list the average hydrogen density along the line of sight, $\bar{n}_{H\,I} = N_{H\,I}/r$. From Figure 5 one can see that the bulk of the absorbing gas cannot be extended along the line of sight by more than the distance $d \simeq 50$ pc beween θ Cen and HD 129685. The filling factor for this gas, $f < d/r$, can be used to derive an upper limit to the fractional ionization $x = n_e/n_{H\,I} = f n_e/\bar{n}_{H\,I}$. By using the upper value for the electron density, $n_e + \epsilon_{n_e}$, we find $x < 0.13$ for the warm gas in front of ζ Cen and $x < 0.07$ for η Cen. The fractional ionization of this gas is therefore lower than that predicted by McKee & Ostriker (1977) for the warm neutral constitutent of the ISM, $x \simeq 0.15$.

The local electron densities derived toward ζ Cen and η Cen are very similar to the space-averaged values derived by means

of pulsar dispersion measures in the LISM (Reynolds 1990). For instance, the electron densities found toward PSR 0823+26 and PSR 0950+08 are $n_e \simeq 0.05$ cm^{-3} and $n_e \simeq 0.02$ cm^{-3}, respectively. According to Reynolds (1990), the lower value of n_e toward PSR 0950+08 could just be a consequence of the relatively high fraction of line of sight within the Local Bubble. In fact, the volume density within the bubble is so low ($n \approx 10^{-3}$ cm^{-3}) that it cannot give a significant contribution to the observed column density of electrons. Sciama (1990) has advanced a similar explanation for the line of sight toward PSR 1451−68 ($n_e \simeq 0.02$ cm^{-3}; Bailes et al. 1990), suggesting that outside very low-density interstellar bubbles the gas responsible for the pulse dispersion should be characterized by a local electron density as high as $n_e \simeq 0.05$ cm^{-3}. Our local electron densities are consistent with such a value of n_e and therefore indicate that the warm neutral gas, in spite of its modest degree of ionization, can contribute significantly to the observed electron column densities in the direction of nearby pulsars, if it occupies a significant fraction of the line of sight.

6. SUMMARY AND CONCLUSIONS

The region of the sky in the range of Galactic coordinates $310° \leq l \leq 330°$ and $15° \leq b \leq 25°$, close to the center of Loop I, has been investigated in a study of the LISM by means of optical and ultraviolet absorption lines.

We have searched for the interstellar components found by LVF within $\simeq 20$ pc of the Sun in the same general direction of the sky. We confirm the presence of the component *P*, with five detections in our field. This component is rather patchy, with inhomogeneities on a scale of $\simeq 0.5$ pc. We cannot confirm the presence of the other two components, *A* and *O*, which according to LVF are located within $\simeq 5$ pc, and of the component *I*, which lies within $\simeq 20$ pc. The Na I/Ca II ratio is less than 1 for the component *P*, and we find evidence from literature data that this is true also for the components *I* and *A*. In agreement with what is expected from the Routly-Spitzer effect, these low Na I/Ca II ratios are associated to high-velocity gas ($V_{LSR} \geq 20$ km s^{-1}), at least in the case of the components *P* and *I*. In the component *I* this effect is hidden, at first sight, by the low projected velocity along the line of sight, but it becomes evident if one considers the modulus of the LSR velocity vector.

The most intense absorptions observed in our optical spectra are produced in gas flowing according to the simple kinematical model suggested by Crutcher (1982). This gas is not homogeneous, since it is characterized by a relatively broad range of column densities, Na I/Ca II ratios, and temperatures. The global velocity vector derived by Crutcher (1982) must be therefore considered a sort of average of velocity vectors of different clumps of gas in the LISM. A similar conclusion was advanced by LVF for the nearby clouds embedded in the Local Bubble, and is extended here to more distant gas located at the boundary of the soft X-ray emitting cavity around the Sun. The Crutcher components generally have Na I/Ca II ratios greater than 1, indicating that grain disruption did not occur, or was very inefficient, during the acceleration of this gas up to the velocity of Crutcher's flow.

The three-dimensional distribution of the interstellar gas in our field has been investigated from an analysis of our UV spectra combined with literature data. We find a two orders of magnitude increase in the H I column density between 15 and 65 pc, followed by a rather constant value at larger distances. This result constrains the distance to the boundary of the Local Bubble in the direction toward the center of Loop I, and it indicates that beyond such boundary our lines of sight are entering another cavity of very low-density gas. The latter conclusion is confirmed by the lack of new interstellar components detected in our optical spectra beyond about 70 pc. The cavity beyond the boundary is identified with the Loop I Bubble on the basis of the scenario proposed by Iwan (1980) and by Cox & Reynolds (1987). Within this framework, the O VI detections toward ζ Cen and ϕ Cen (Jenkins 1978) can be attributed to hot gas located either in the Local Bubble or in the Loop I Bubble. The three-dimensional gas distribution implied by our results supports the model for the production of the observed soft X-ray background based on thermal emission (Snowden et al. 1990).

We have combined column densities of UV (Mg I, Zn II) and optical (Na I) species to investigate the physical state of the gas at the boundary of the Local Bubble intercepted by our lines of sight. The temperatures have been estimated by comparing the observed Mg I/Na I ratios with the theoretical ones, under the assumption of ionization equilibrium. Also the observed Zn II/Na I ratios have been used to obtain some qualitative indication on the temperatures. In the case of HD 129685 we have used the line-of-sight velocity dispersion of the Na I lines to derive an upper limit on *T*. We find evidence of warm gas in front of ζ Cen ($T \simeq 6.0 \times 10^3$ K) and η Cen ($T \simeq 6.9 \times 10^3$ K) and of colder gas toward HD 129685 ($T < 2.7 \times 10^3$ K) and probably HD 119921. These temperature values have been used to derive the electron density in the warm gas by means of an analysis of the Zn II/Mg I ratio, employed here for the first time. The resulting electron densities in the directions of ζ Cen ($n_e \simeq 0.04$ cm^{-3}) and η Cen ($\simeq 0.03$ cm^{-3}), once combined with the hydrogen densities in the same lines of sight, allow the possibility of a modest ionization fraction ($x < 0.1$). These electron densities are in good agreement with the space averaged densities found by means of pulsar dispersion measures in the solar vicinity, suggesting that this kind of warm gas is capable of giving a substantial contribution to the observed electron column densities in the interstellar space, if the warm gas has a significant volume filing fraction.

We thank M. Arnaud and R. Rothenflug for making available to us their code for the computation of the ionization balance in the ISM, Prof. D. Sciama for helpful discussions, and the referee for clarifying comments. This work has been carried out during the stay of M. C. at the OAT, thanks to a grant of Gobierno de Canarias and Caja Gnl. de Ahorros de Canarias.

REFERENCES

Arnaud, M., & Rothenflug, R. 1985, A&AS, 60, 425
Bailes, M., Manchester, R. N., Kesteven, M. J., Norris, R. P., & Reynolds, J. E. 1990, Nature, 342, 240
Berkhuijsen, E. M., Haslam, C. G. T., & Salter, C. J. 1971, A&A, 14, 252
Bertaux, J. L. 1984, in IAU Colloquium 81, Local Interstellar Medium (NASA CP-2345), p. 3
Bohlin, R. C., Hill, J. K., Jenkins, E. B., Savage, B. D., Snow, T. P., Spitzer, L., & York, D. G. 1983, ApJS, 51, 277
Bohlin, R. C., Savage, B. D., & Drake, J. F. 1978, ApJ, 224, 132
Bruhweiler, F., & Vidal-Madjar, A. 1987, in Exploring the Universe with the *IUE* Satellite, ed. Y. Kondo (Dordrecht: Reidel), p. 467
Cox, D. P., & Reynolds, R. J. 1987, ARA&A, 25, 303

Crutcher, R. M. 1982, ApJ, 253, 82
de Boer, K. S., Jura, M. A., & Shull, J. M. 1987, in Exploring the Universe with the *IUE* Satellite, ed. Y. Kondo (Dordrecht: Reidel), p. 485
Ferlet, R., Vidal-Madjar, A., & Gry, C. 1985, ApJ, 298, 838
FitzGerald, M. P. 1970, A&A, 4, 234
Frisch, P. 1981, Nature, 293, 377
Genova, R., Molaro, P., Vladilo, G., & Beckman, J. E. 1990, ApJ, 355, 150
Gondhalekar, P. M., Phillips, A. P., & Wilson, R. 1980, A&A, 85, 272
Grenier, S., Gomez, A. E., Jaschek, C., Jaschek, M., & Heck, A. 1985, A&A, 145, 331
Grevesse, N. 1984, Phys. Scripta, T8, 49
Harris, A. W., & Mas Hesse, J. M. 1986, MNRAS, 220, 271
Hobbs, L. M. 1983, ApJ, 265, 817
Hoffleit, D., & Jaschek, C. 1982, The Bright Star Catalogue (4th revised ed.; New Haven: Yale University Observatory)
IHAP User Manual 1983 (Munich: ESO)
Iwan, D. 1980, ApJ, 239, 316
Jacobs, V. L. 1985, ApJ, 296, 121
Jenkins, E. B. 1978, ApJ, 219, 845
Jenkins, E. B., Drake, J. F., Morton, D. C., Rogerson, J. B., Spitzer, L., & York, D. G. 1973, ApJ, 181, L122
Keenan, F. P. 1984, MNRAS, 206, 449
Keenan, F. P., Bates, B., & Catney, M. G. 1986, in New Insights in Astrophysics (ESA SP-263), p. 565
Lallement, R., Vidal-Madjar, A., & Ferlet, R. 1986, A&A, 168, 225 (LVF)
Landsman, W.B., Henry, R. C., Moos, H. W., & Linsky, J. L. 1984, ApJ, 285, 801
McCammon, D., Burrows, D. N., Sanders, W. T., & Kraushaar, W. L. 1983, ApJ, 269, 107
McKee, C. F., & Ostriker, J. P. 1977, ApJ, 218, 148
Morton, D. C. 1978, ApJ, 222, 863
Morton, D. C., & Smith, W. H. 1973, ApJS, 26, 333
Murray, M. J., Dufton, P. L., Hibbert, A., & York, D. G. 1984, ApJ, 282, 481
Paresce, F. 1984, A&A, 89, 1022
Péquignot, D., & Aldrovandi, S. M. V. 1986, A&A, 161, 169
Pettini, M., Boksenberg, A., Bates, B., McCaughan, R. F., & McKeith, C. D. 1977, A&A, 61, 839
Phillips, A. P., Pettini, M., & Gondhalekar, P. M. 1984, MNRAS, 206, 337
Pottasch, S. R. 1972, A&A, 20, 245
Reynolds, R. J. 1990, ApJ, 348, 153
Routly, P. M., & Spitzer, L., Jr. 1952, ApJ, 115, 227
Sciama, D. 1990, Nature, 346, 40
Shull, J. M., & Van Steenberg, M. E. 1982, ApJS, 48, 95
———. 1985, ApJ, 294, 599
Shull, J. M., Van Steenberg, M. E., & Seab, C. G. 1983, ApJ, 271, 408
Siluk, R. S., & Silk, J. 1974, ApJ, 192, 51
Snowden, S. L., Cox, D. P., McCammon, D., & Sanders, W. T. 1990, ApJ, 354, 211
Unsöld, A. 1955, Phisik der Sternatmosphären (2nd ed.; Berlin: Springer)
Vidal-Madjar, A., Ferlet, R., Gry, C., & Lallement, R. 1986, A&A, 155, 407
Weaver, H. 1979, in IAU Symposium 84, The Large Scale Characteristics of the Galaxy, ed. W. B. Burton (Dordrecht: Reidel), p. 295
Walborn, N. R. 1972, AJ, 77, 312